Illuminating N-acylethanolamine biosynthesis with new chemical tools

Mock, E.D.

Chapter 7

Summary and future prospects

In this thesis, the discovery and optimization is described of chemical tools to study the *N*-acylethanolamine (NAE) biosynthetic pathway. In particular, two enzymes – *N*-acylphosphatidylethanolamine phospholipase D (NAPE-PLD) and phospholipase A and acyltransferase 2 (PLAAT2) – were targeted, which produce NAEs or their NAPE precursors, respectively. To identify inhibitors for these enzymes, high-throughput screening (HTS) or focused-library screening approaches were applied. Using structure-activity relationship (SAR) studies, initial hits were optimized to potent inhibitors, possessing cellular and/or *in vivo* efficacy. On-target confirmation was achieved by employing photoaffinity labeling (PAL) or activity-based protein profiling (ABPP). Cellular and/or *in vivo* activity of the described inhibitors was confirmed with targeted lipidomics experiments. Finally, the herein described NAPE-PLD inhibitor **LEI-401** demonstrated analgesic effects in mice that could be of therapeutic value and will be the focus of ongoing research.

In **Chapter 1**, an overview is provided of the metabolism and bioactivities of NAEs. NAEs are a family of lipid signaling molecules that includes *N*-palmitoylethanolamine

(PEA), *N*-oleoylethanolamine (OEA), *N*-arachidonoylethanolamine (anandamide or AEA) and *N*-docosahexaenoylethanolamine (DHEA). The NAEs exert their signaling role through activation of several receptors in the brain as well as in the periphery. Over the past three decades a growing list of G protein-coupled receptors (GPCRs), ion channels and nuclear receptors were found to be targeted by specific NAEs. Most famously, anandamide was discovered in 1992 as the first endogenous agonist for the cannabinoid CB_1 receptor, and was therefore coined an endogenous cannabinoid or endocannabinoid.[1] Continuing studies have shown that anandamide is also an agonist for the CB_2 receptor and transient receptor potential vanilloid receptor 1 (TRPV1) and, as a result, AEA is considered an endovanilloid as well.[2] Many biological activities have been attributed to anandamide, which include pain reduction[3], appetite stimulation[4], regulation of fertility[5], neuroprotection[6], memory consolidation[7] and anti-depressive[8] and anti-anxiety[9] functions.

Furthermore, **Chapter 1** discusses the therapeutic opportunities of modulating the endogenous NAE tone including AEA, with a specific focus on depleting NAE levels. NAEs and their metabolic enzymes were found to be aberrantly regulated and associated with disease severity in obesity[10], metabolic syndrome[11], hepatic[12] and blood[13] cancers and liver cirrhosis[14]. Pharmacological inhibition of CB_1 and other NAE receptors has shown efficacy for these conditions in clinical or pre-clinical studies. Unfortunately, antagonism of brain CB_1 receptors triggered adverse psychiatric side effects, leading to the market withdrawal of the obesity drug rimonabant. Peripheral CB_1 receptor blockade is currently being investigated as a new therapeutic option.[15] Alternatively, targeting the biosynthetic enzymes of NAEs may be a viable strategy for treatment of these pathological conditions. A potential advantage of depleting NAE signaling could be that this leads to partial antagonism, since most NAE receptors have other endogenous lipid agonists, thereby providing a fine-tuned therapeutic effect. So far, no inhibitors are available that allow reduction of NAE levels in cellular or animal models, making this an underexplored area of research. New pharmacological tools that block NAE biosynthetic enzymes are therefore needed to enable the study of NAE signaling in health and disease models.

7.1 Development of *in vivo* active NAPE-PLD inhibitors

Whereas the degradation of anandamide by the enzyme fatty acid amide hydrolase (FAAH) has been well studied by genetic and pharmacological means, the exact conditions that govern AEA biosynthesis are not completely clear.[16] The zinc hydrolase NAPE-PLD is considered to be the main enzyme that produces NAEs including AEA. However, mouse

NAPE-PLD knock-out (KO) models have shown varying degrees of anandamide reduction, with only two out of three studies reporting decreased brain AEA levels.[17-19] Compensatory mechanisms or other NAE biosynthetic pathways have therefore been suggested to take over the role of NAPE-PLD.[17] To study anandamide signaling in closer detail, pharmacological tools are necessary that allow acute inhibition of its biosynthesis. At present, no such tools are available for NAPE-PLD to modulate its activity in cells or whole animals.

In **Chapter 2**, new chemotypes that inhibit NAPE-PLD were sought by screening a large compound collection using high-throughput screening (HTS). A fluorescence-based NAPE-PLD activity assay was optimized to be HTS-compatible. The assay utilizes the fluorescence-quenched substrate PED6, which is hydrolyzed at the phosphodiester bond by NAPE-PLD. This releases the fluorophore from the quencher, providing a fluorescence increase proportional to the enzymatic activity. In the HTS campaign, a library of ~350,000 compounds was screened at 10 μM (single point measurement) in a 1536-well format. After hit validation, dose-response experiments and two deselection assays, which filtered for zinc chelators and quenchers, five hit compounds were identified. Owing to its favorable submicromolar potency, physicochemical properties and synthetic accessibility, pyrimidine-4-carboxamide **1** (Figure 1) was resynthesized and its activity confirmed in the PED6 assay. Off-target profiling for the receptors and enzymes of the endocannabinoid system (ECS) showed that **1** is selective for NAPE-PLD *in vitro*. Thus, compound **1** constituted a new scaffold with potential for further optimization to obtain *in vivo* active NAPE-PLD inhibitors.

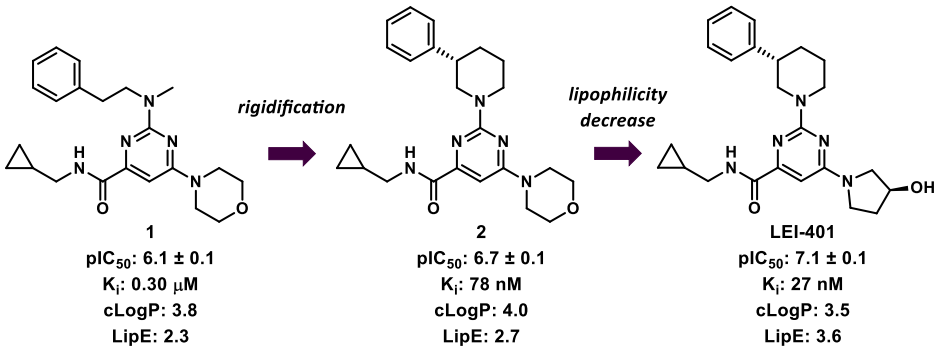

Figure 1. Strategy employed to optimize hit compound **1** to potent NAPE-PLD inhibitor **LEI-401**. cLogP was calculated using Chemdraw 15. Lipophilic efficiency (LipE) = pIC_{50} - cLogP.

A structure-activity relationship (SAR) study was performed in **Chapter 3** to improve the potency of hit compound **1** for NAPE-PLD. Synthesis and activity testing of 104 analogues of **1** resulted in the identification of **LEI-401**, a nanomolar potent NAPE-PLD inhibitor. Conformational restriction of the *N*-methylphenethylamine of **1** to an (*S*)-3-phenylpiperidine increased the potency by 4-fold (compound **2**, Figure 1). Modification of the morpholine of **1** for an (*S*)-3-hydroxypyrrolidine further improved the inhibitory activity by 3-fold and simultaneously reduced the lipophilicity. **LEI-401** possessed favorable physicochemical (drug- like) properties such as lipophilic efficiency (LipE) and topological polar surface area (tPSA), making it suitable for cellular and *in vivo* studies.

In **Chapter 4**, target engagement of **LEI-401** was investigated to verify its binding interaction with NAPE-PLD in live cells. A photoaffinity labeling (PAL) approach was chosen, which is an established technique to identify protein-drug interactions for metallo-hydrolases.[20] Here, a photoaffinity probe covalently binds its intended target upon UV-irradiation, allowing protein identification by gel- or chemical proteomics-based methods. The probe-protein labeling can be displaced with a competitor, which provides proof of target engagement. Two strategies were investigated for the development of NAPE-PLD photoprobes. The first strategy involved synthesis of NAPE substrate mimics, incorporating a diazirine photocrosslinker, a stabilized phosphodiester bioisostere and an alkyne ligation handle. Biological evaluation revealed that these probes had low affinity for NAPE-PLD in an *in vitro* activity assay and were not able to label NAPE-PLD in human embryonic kidney (HEK293T) cells transiently transfected with this enzyme. A second strategy took advantage of the NAPE-PLD inhibitor library (as described in Chapter 3) to guide the design of pyrimidine-4-carboxamide-based photoaffinity probes. Photoprobe **3** displayed submicromolar potency for NAPE-PLD and could efficiently label this enzyme in overexpressing HEK293T cells (Figure 3). Gel- and chemical proteomics-based competition experiments provided evidence of NAPE-PLD target engagement by **LEI-401** in live cells.

In **Chapter 5**, **LEI-401** was profiled in cellular and animal models. First, it was determined that **LEI-401** is selective for NAPE-PLD over the receptors and enzymes in the ECS. Targeted lipidomics measurements in mouse neuronal cells revealed that **LEI-401** reduces NAE levels in wild-type (WT), but not in NAPE-PLD KO cells. Encouraged by this result, **LEI-401** was tested in C57BL/6J mice, where it showed favorable pharmacokinetic (PK) properties. Two hours after a single intraperitoneal dose (30 mg/kg), **LEI-401** displayed high brain and plasma levels. A time- and dose-dependent reduction of brain anandamide levels was observed, matching the **LEI-401** PK profile. This indicated that **LEI-401** is an *in vivo* active, brain penetrant NAPE-PLD inhibitor and emphasized the role of NAPE-PLD in brain AEA production. To assess the pharmacological effect of acute brain

anandamide reduction, **LEI-401** was profiled in several behavioral assays. This revealed that **LEI-401** elicited antinociceptive, hypomotile and hypothermic effects in C57BL/6J mice, which were not mediated by the CB_1 receptor. Furthermore, in a mouse model of inflammatory pain, **LEI-401** was able to fully reverse lipopolysaccharide (LPS)-induced allodynia. Collectively, these data show that **LEI-401** possesses analgesic properties that could be of therapeutic use. Future studies with **LEI-401** in NAPE-PLD KO mice are necessary to establish whether these behavioral effects are NAPE-PLD dependent.

7.1.1 Towards improved *in vivo* active NAPE-PLD inhibitors.

In **Chapters 4** and **5**, **LEI-401** displayed cellular target engagement, high brain penetration and *in vivo* efficacy. While **LEI-401** will be tested in various disease models in mice as a 1^{st}-generation centrally active NAPE-PLD inhibitor, its high dosing (30 mg/kg) may give rise to off-target interactions and toxicity issues, especially after repeated administration. Further optimization of the inhibitor scaffold is therefore required. This can be accomplished by improving drug properties such as potency, selectivity, solubility and metabolic stability. Ideally, a drug candidate possesses single digit nanomolar potency, a LipE greater than 5 and a half-life ($t_{1/2}$) of 12 h by oral dosing.[21,22] For **LEI-401** these parameters are: $K_{i,NAPE\text{-}PLD}$ = 27 nM (human), 180 nM (mouse); LipE = 3.68 (human), 2.89 (mouse); $t_{1/2}$ = 2.7 h.

In Figure 2, an overview is given of potential strategies to improve the **LEI-401** inhibitor structure. The SAR-analysis described in **Chapter 3** showed that the *ortho* position on the phenyl ring was suitable for modification. Bulky biphenyl and diphenyl ether derivatives displayed inhibitory activities equivalent to the unsubstituted phenyl of **1**. This suggests that polar groups such as nitrile and methoxy or small heterocycles can be accommodated at this position, improving the solubility and LipE. Incorporation of a *para*-fluoro substituent on the phenyl ring can increase the metabolic stability by reducing compound degradation in the liver.[23] Additional sites that can be explored are the 2-, 4- and 6-position on the piperidine ring, as well as the 2-, 4- and 5-position of the pyrrolidine, where additional space was found in the SAR. However, it has to be taken into account that for optimal brain exposure the tPSA should not exceed 90 $Å^2$, limiting the possible polar modifications. Optimization of the core scaffold can be explored with annulated bicyclic rings. Finally, generating a co-crystal structure of **LEI-401** in the reported NAPE-PLD crystal structure will shed light on its binding mode and aid future inhibitor development.

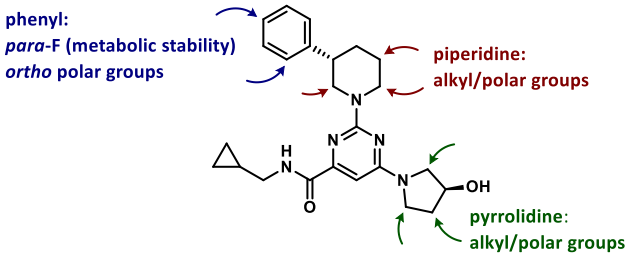

Figure 2. Possible strategies to improve the potency and pharmacokinetic profile of **LEI-401**.

Besides targeting NAPE-PLD in the brain, specifically inhibiting NAPE-PLD in the periphery could be of therapeutic use as well. For example, modulating peripheral levels of OEA and AEA may be beneficial in pathological conditions such as leukemia[13] and obesity[11]. An often employed strategy for developing peripherally restricted inhibitors is by increasing the tPSA, which should be between 90 and 120 Å^2 to minimize brain exposure, while still allowing passive plasma membrane diffusion.[24] This may be accomplished by introducing polar substituents (e.g. H-bond donors and/or acceptors) on the **LEI-401** structure as depicted in Figure 2.

7.1.2 Photoaffinity labeling of endogenous NAPE-PLD and looking for LEI-401 off-targets. In **Chapter 4**, photoprobe **3** was effective to show target binding of **LEI-401** with NAPE-PLD in HEK293T cells overexpressing this enzyme. Efforts to label endogenous NAPE-PLD in different cell lines (HEK293T, Neuro-2a, RAW264.7) were unsuccessful so far. In mock-transfected HEK293T cells, a fluorescent band was visible at the estimated height of NAPE-PLD (Chapter 4, Figure 8A-B) and could be competed out by **LEI-401**. However, in subsequent label-free proteomics experiments no NAPE-PLD peptides were detected. To boost the detection sensitivity in a pulldown experiment, different strategies can be employed. Firstly, increasing the potency of the photoprobe can improve photocrosslinking efficiency. This can be achieved by generating new photoprobes that closely mimic the potent inhibitor **LEI-401**, for example compound **4** (Figure 3). Compound **5** could exploit a lipophilic binding pocket that was discovered during the SAR-analysis (Chapter 3), that allowed incorporation of the large *N*-methylphenethylamine group. Alternatively, the efficiency of the azide-alkyne click reaction may be improved. In Chapter 3, it was found that the alkyne resides in a small hydrophobic pocket, suggesting that it may be buried in the protein structure. Therefore, positioning the alkyne handle in more available positions (*e.g.* compounds **6** and **7**) could make the click reaction more efficient and improve protein detection.

Apart from labeling NAPE-PLD, the photoaffinity probes developed in **Chapter 4** can aid in the discovery of **LEI-401** off-targets. In Chapter 5, **LEI-401** reduced 2-AG and other monoacylglycerol (MAG) levels in both WT and NAPE-PLD KO Neuro-2a cells. In the brains of C57BL/6J mice, **LEI-401** also significantly decreased 2-AG levels in a dose-dependent manner, which is known to cause anti-inflammatory effects.[25] It is possible that the **LEI-401**-induced AEA depletion in the brain generated a crosstalk with 2-AG metabolism. Similar interconnected endocannabinoid changes in the brains of mice have been reported for FAAH and diacylglycerol lipase-α (DAGLα) inhibitors, the enzymes that hydrolyze AEA or produce 2-AG, respectively.[25,26] Alternatively, **LEI-401** could exert cellular and *in vivo* effects through one or more yet unknown protein targets. Photoaffinity labeling coupled with chemical proteomics is an established method for protein target identification of small molecules and natural products.[27,28] In recent years, technological advances have also enabled determination of the site of protein photocrosslinking.[29] To pinpoint the binding site, most often cleavable linkers are used, which facilitate enrichment of probe-labeled peptides.[30] Screening various cell lines using the PAL protocol described in Chapter 4, *e.g.* cell lines involved in the inflammatory response, is thus a suitable approach to find additional targets of **LEI-401**.

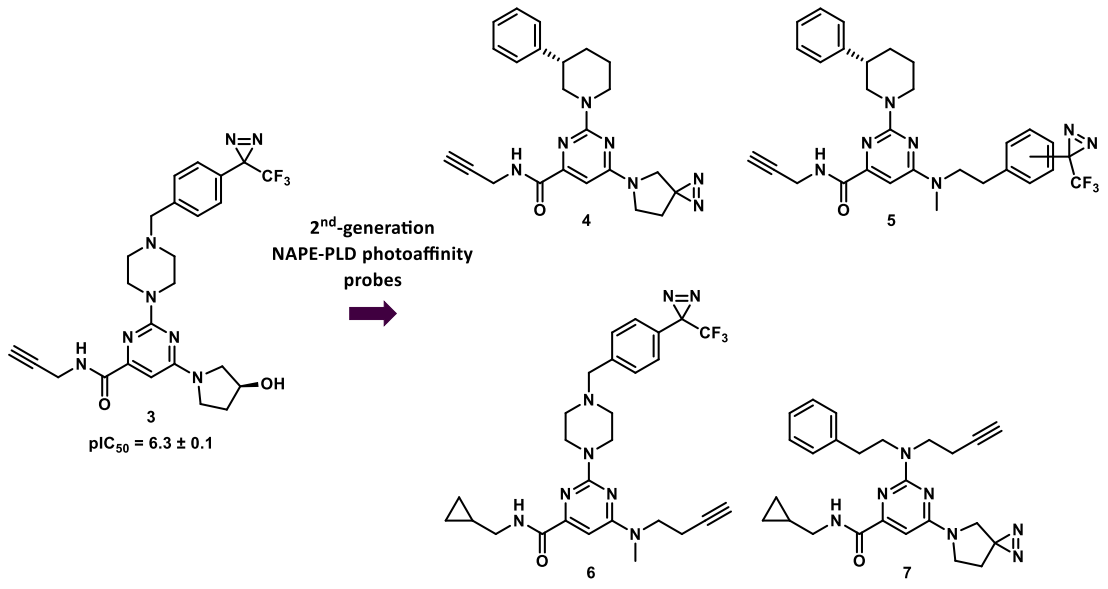

Figure 3. Structures of NAPE-PLD photoprobe **3** and suggested 2nd-generation NAPE-PLD PAL probes **4-7**.

7.2 Development of Ca^{2+}-independent NAPE biosynthesis inhibitors

It is generally assumed that the rate-limiting step in NAE biosynthesis is the formation of NAPEs catalyzed by *N*-acyltransferase (NAT) activity.[31,32] Besides the canonical Ca^{2+}-dependent NAPE-producing pathway, in recent years, new Ca^{2+}-independent enzymes have been identified.[16] In particular, PLAAT2 was reported to have high *N*-acyltransferase activity *in vitro*.[33] So far, no pharmacological tools have been reported that allow interrogation of cellular PLAAT2 activity. In **Chapter 6**, a recently reported ABPP assay[34] was used to screen a focused library of lipase inhibitors for PLAAT2 activity. Compound **8** was identified as the most potent hit of several α-ketoamide inhibitors that were effective against PLAAT2 (Figure 4). SAR-analysis of the α-ketoamide scaffold culminated in optimized inhibitor **LEI-301**, which had a 13-fold increase in potency compared to **8**. **LEI-301** exhibited similar inhibitory activities for the other members of the PLAAT family, but was selective over the receptors and enzymes of the ECS. Human osteosarcoma (U2OS) cells transiently transfected with PLAAT2 showed a remarkable increase in NAE content, which was significantly reduced when treated with **LEI-301**. In control cells, NAE levels were not affected by **LEI-301** treatment, indicating that the compound inhibited PLAAT2 in live cells. The work described in this chapter confirms that PLAAT2 can contribute to NAE biosynthesis. Furthermore, α-ketoamides are presented as a novel class of inhibitors that enable the study of NAE and NAPE signaling in cellular systems.

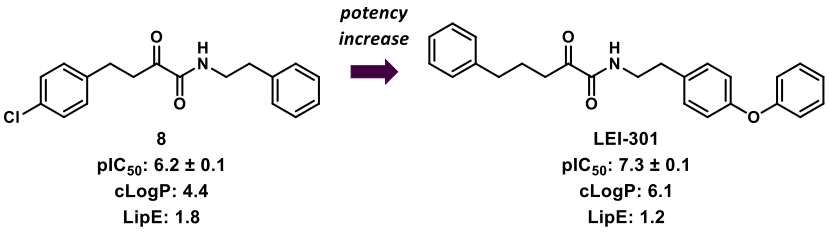

8
pIC_{50}: 6.2 ± 0.1
cLogP: 4.4
LipE: 1.8

LEI-301
pIC_{50}: 7.3 ± 0.1
cLogP: 6.1
LipE: 1.2

Figure 4. Structures and physicochemical parameters of α-ketoamide screening hit **8** and optimized PLAAT2 inhibitor **LEI-301**. cLogP was calculated using Chemdraw 15. Lipophilic efficiency (LipE) = pIC_{50} - cLogP.

7.2.1 Towards selective and *in vivo* active PLAAT2 inhibitors.

LEI-301 was identified in **Chapter 6** as a potent inhibitor of PLAAT2 inhibitor with cellular activity. However, due to its high lipophilicity and low LipE, **LEI-301** is not suitable for *in vivo* use. Modification of the α-ketoamide scaffold is therefore required to improve these

properties. Possible sites that merit further optimization are highlighted in Figure 5. SAR-analysis and molecular docking experiments revealed that introduction of a *para*-phenoxy substituent on the phenethylamine group gave a boost in potency due to π-π stacking with a tyrosine side chain. By placing the phenoxy group on the *ortho* or *meta* positions, the optimal site for the π-interaction can be probed. Also, different heterocyclic or biphenyl motifs should be explored. Recently, a patent describing α-ketoamide inhibitors for PLAAT3 showed that heteroatoms and alkyl groups can be incorporated across the alkyl chain (for example compound **9**, Figure 5).[35] Because of the similar potency of **LEI-301** for PLAAT3 and PLAAT2 and the high homology between these two enzymes (69%), **LEI-301** could also benefit from heteroatom and alkyl modifications on the alkyl chain, thereby decreasing the lipophilicity. Replacing the phenyl group on the ketone side for a CF_3 could improve the solubility, while the activating effect on the ketone compensates for the loss of the aromatic interaction. Finally, the reported crystal structures for PLAAT2 and PLAAT3 may guide the development of family member-selective inhibitors, using molecular docking or co-crystal structures.[36,37]

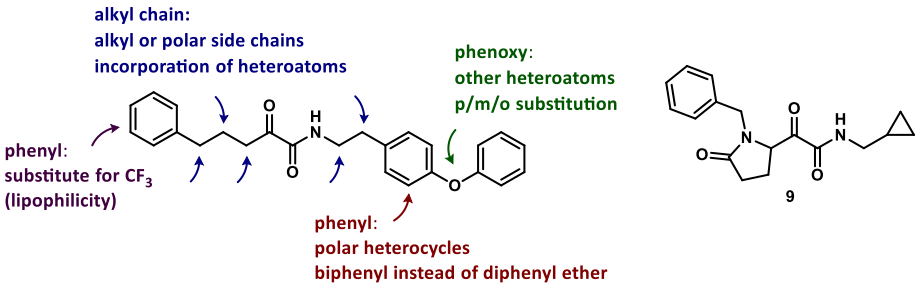

Figure 5. Left: possible strategies to improve the potency and physicochemical properties of **LEI-301**. Right: structure of reported PLAAT3 inhibitor **9**.

7.2.2 Novel covalent α-ketoamide inhibitors and ABPs for the PLAAT family.

The fluorescent activity-based probe (ABP) MB064 has enabled visualization of PLAAT family members in lysates of transiently transfected cells, as well as endogenous PLAAT3 activity in brown and white adipose tissue.[34] So far, efforts to confirm target engagement of the PLAAT enzymes by chemical proteomics using the corresponding biotin probe MB108[38] (Figure 6A) have been unsuccessful. A possible explanation could be the thioester linkage that is formed between the active site cysteine of the PLAAT members and the β-lactone of the ABP. Thioesters may be susceptible to hydrolysis or transthioesterification with DTT during the pulldown protocol.[39] Therefore, when MB108

is used in chemical proteomics experiments with the aim of identifying PLAAT enzymes, strictly non-reducing conditions should be employed. Alternatively, the design of new ABPs that produce a stable covalent linkage with the PLAAT enzymes could be investigated. For example, ABPs for cathepsin and caspase cysteine proteases have used the phenoxymethylketone (PMK) motif as electrophilic trap, which generates a stable thioether bond.[40-42] Incorporation in the α-ketoamide scaffold yields PMK **10**, which could represent a possible broad-spectrum ABP for PLAAT enzymes (Figure 6B). A proposed synthesis of probe **10** is depicted in Scheme 1. Alkylation of Boc-protected tyramine **11** with propargyl bromide affords **12**. Boc deprotection and amide coupling with β-chlorolactic acid gives **14**. Subsequent DMP oxidation generates chloromethylketone **15**, which can be converted to the PMK **10** using 2,3,5,6-tetrafluorophenol and potassium fluoride.[40]

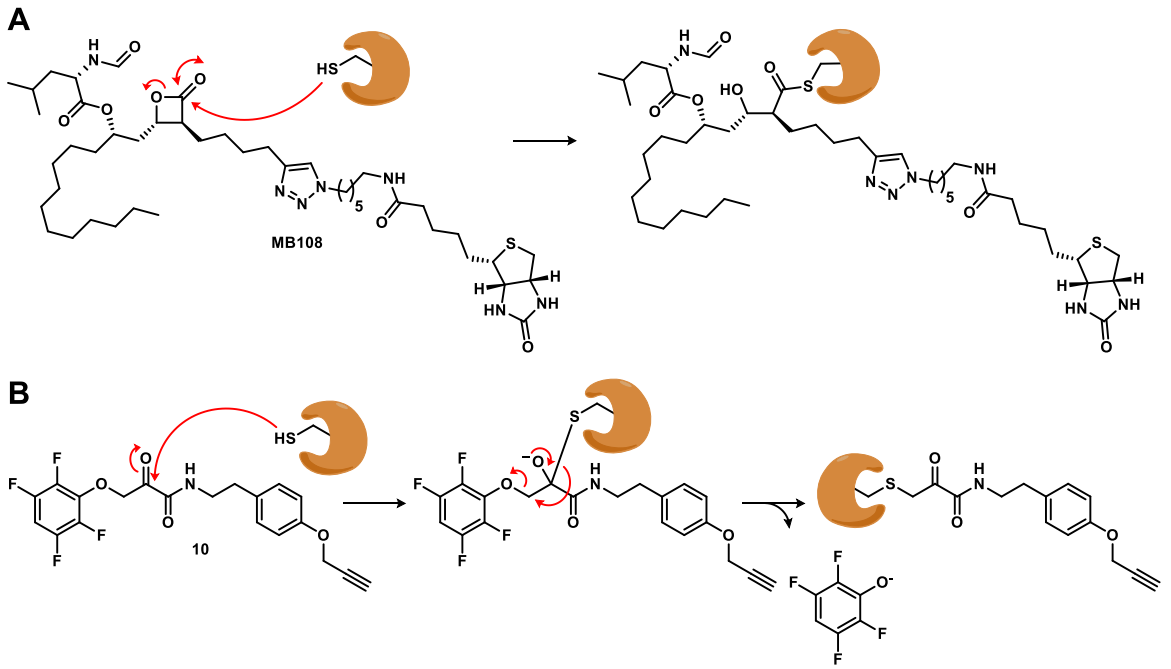

Figure 6. A) Proposed mechanism of activity-based probe (ABP) MB108 with PLAAT enzymes, which produces a labile thioester. **B**) Suggested structure of a phenoxymethylketone ABP **10** that targets the PLAAT family and forms a stable thioether bond.

An ABP that is specific for the PLAAT family will help to reveal the endogenous activities of the family members in different tissues. This is specifically relevant for PLAAT2 of which the physiological role is yet unknown. High expression levels of PLAAT2 were found in organs of the human digestive system, including liver, kidney, small intestine and

colon.[43,44] PLAAT2 could therefore contribute to NAE biosynthesis in the gut, where anandamide and OEA are involved in food intake and satiety.[45,46] The described inhibitors and ABPs will enable further investigation of these questions.

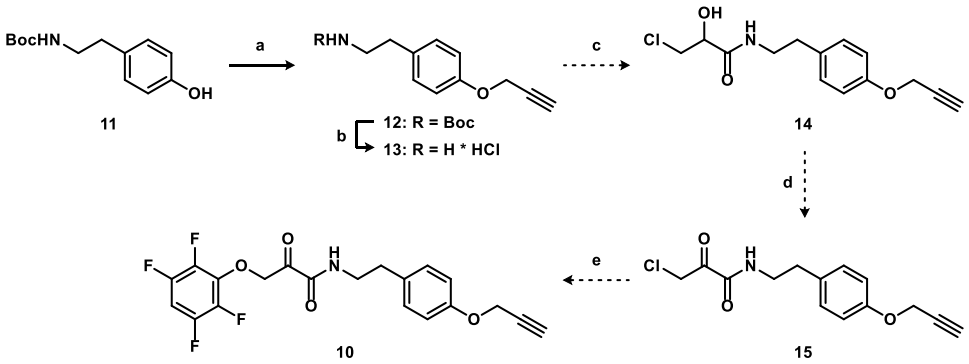

Scheme 1. Synthetic route towards putative activity-based probe **10** for the PLAAT family. Reagents and conditions: a) propargyl bromide, K_2CO_3, DMF, rt, 92%; b) HCl, dioxane, rt, 99%; c) β-chlorolactic acid, HATU, DiPEA, DMF; d) Dess-Martin periodinane, DCM; e) 2,3,5,6-tetrafluorophenol, KF, DMF.

7.3 Identification of NAPE protein targets using photoaffinity labeling.

In **Chapter 1**, NAPEs are highlighted as an underexplored class of phospholipids in human physiology. NAPEs are primarily considered to be precursors for NAEs.[16] In recent years, multiple studies have suggested that NAPEs have a bioactive role themselves.[47,48] NAPEs have a reported membrane-stabilizing role and possess fusogenic properties.[49-52] In mammals, NAPE levels are highly elevated during cellular injury in several tissues, such as brain and heart, presumably due to an influx of Ca^{2+}-ions.[53-59] Also in plants, NAPEs accumulate under cellular stress.[60,61] NAPEs are implicated in neuroprotection, anti-inflammation and satiety.[47,48] However, the molecular mechanisms through which NAPEs exert their biological functions are unclear.

A photoaffinity labeling approach was applied to search for protein targets that can explain the putative bioactivities of NAPEs. To this end, NAPE-like photoprobes **16-22** (Figure 7A, synthesis described in Chapter 4) were used to identify covalently bound targets by chemical proteomics. As a model system, the mouse Neuro-2a neuroblastoma cell line was selected, to detect binding partners of NAPEs in the brain. The photolabeling efficiencies of probes **16-22** in this cell line were assessed in a gel-based photoaffinity labeling experiment. 750.000 cells were incubated with the different photoprobes

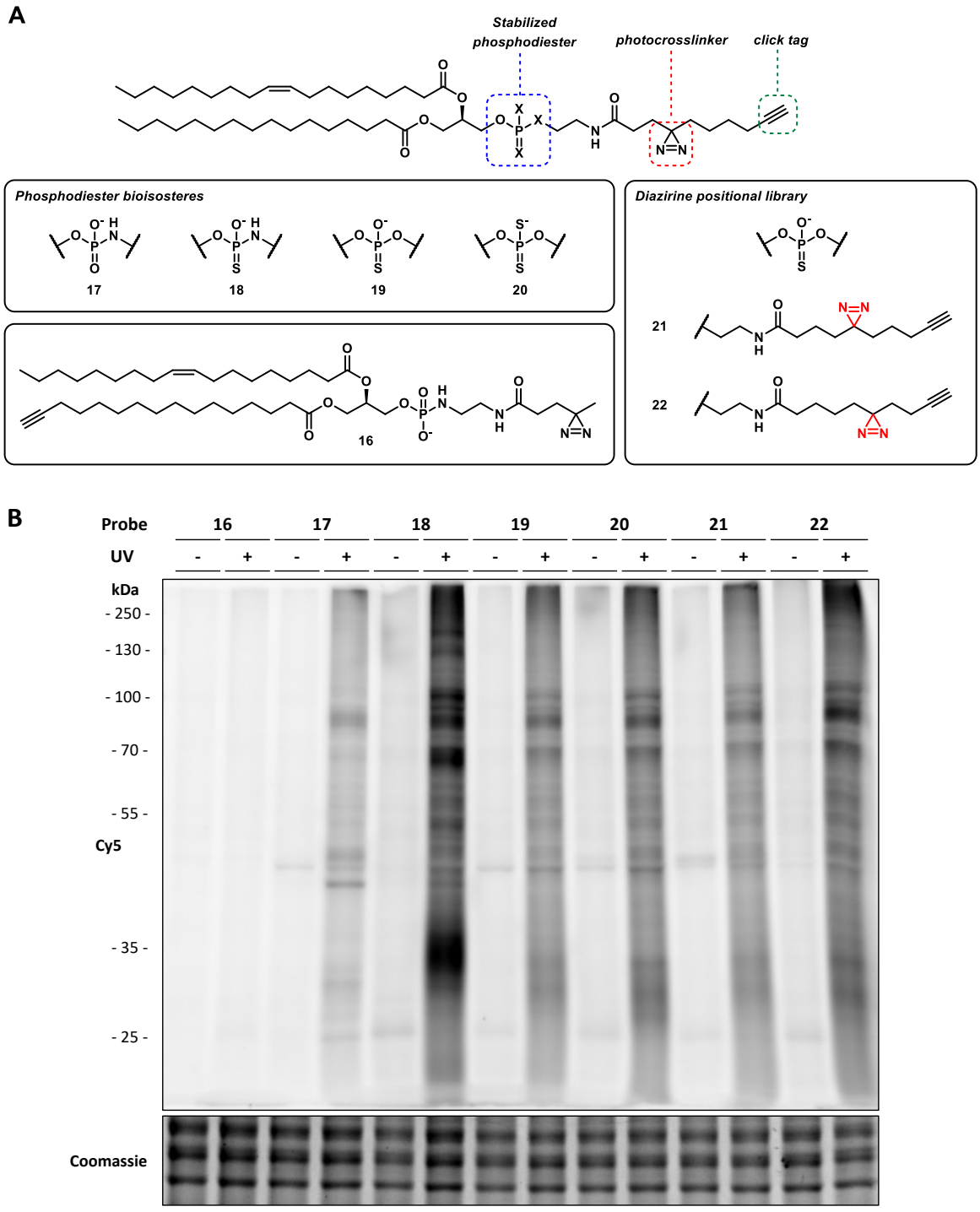

Figure 7. A) Structures of NAPE-based PAL probes **16-22**, which incorporate a stabilized phosphodiester mimic, a photoreactive diazirine and an alkyne ligation handle (synthesis described in Chapter 4). **B**) Photoaffinity labeling of NAPE-like photoprobes **16-22** (20 μM, 30 min) showing UV-dependent labeling of proteins in live Neuro-2a cells.

(20 μM, 30 min) and irradiated with 350 nm UV light for 10 min or kept in the dark as a control. The cells were lysed, clicked with Cy5-N_3 and the proteins were resolved by

sodium dodecyl sulfate polyacrylamide gel electrophoresis (SDS-PAGE). UV-dependent labeling of various proteins was apparent for all probes except for **16**, possibly due to instability of the phosphoramidate moiety (Figure 7B).[62] Thiophosphoramidate probe **18** displayed the highest labeling intensity of all the probes and was therefore selected for further characterization.

To identify the labeled proteins by probe **18** a chemical proteomics experiment was performed (similar workflow as in Chapter 4, Figure 2). Ten million cells were treated with probe **18** (20 μM, 30 min, n = 3 per condition) and were either UV irradiated (350 nm, 10 min) or kept in the dark. The cells were lysed and separated in membrane and cytosol fractions by ultracentrifugation to increase the peptide detection sensitivity. The lysates were clicked with biotin-N_3 and the probe-targeted proteins were enriched with avidin agarose beads, followed by on-bead trypsin digestion. The tryptic peptides were treated with deuterated (heavy) or hydrogen (light) isotopically labeled formaldehyde to allow quantification by reductive dimethylation using MaxQuant software (Figure 8).[63,64] By combining heavy labeled and light labeled peptide fragments with or without UV-irradiation in equal parts (1:1), ratios were obtained of the UV-dependent labeling of the protein target (+UV/-UV intensity) or reproducibility of the experiment (+UV/+UV intensity). Cut-offs for protein target identification were: 1) at least 2 unique peptides, 2) a heavy/light ratio x between $0.5 \leq x \leq 2$ for +UV/+UV intensity, 3) a heavy/light ratio $x \geq 2$ for +UV/-UV intensity and testing for significance ($P < 0.05$) using Student's *t*-test (unpaired, two-tailed) with Benjamini-Hochberg correction (false discovery rate (FDR) 25%).

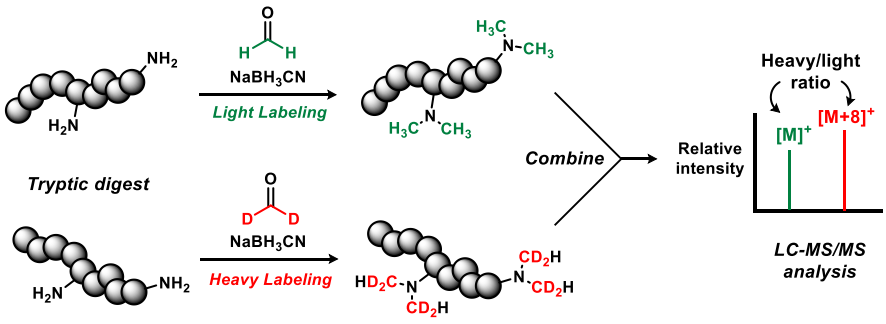

Figure 8. Dimethyl labeling using deuterium (heavy) and hydrogen (light) isotopically labeled formaldehyde allows quantification of peptide fragments.

A total of 162 proteins were identified in this experiment, which gave 17 UV-enriched protein targets (Figure 9A). Of these, four proteins were considered significant: cathepsin D (Ctsd), prosaposin (Psap), Ras-related C3 botulinum toxin substrate 1 (Rac1) and Myb-

binding protein 1a (Mybbp1a or p160) (Figure 9B, Table 1). Cathepsin D was previously reported to be a putative target of aliphatic diazirine photocrosslinkers in human A549 and HeLa cell lines and was therefore not further pursued.[65] A literature search for Psap revealed that it is a precursor for a family of non-enzymatic lipid binding proteins called sphingolipid activator proteins or saposins A-D.[66] Saposins A-D reside in the lysosome where they facilitate the breakdown of sphingolipids and gangliosides by different hydrolases. Of note, proteolysis of prosaposin to the individual saposins can be performed by cathepsin D in the lysosome.[67] To elucidate which form of prosaposin was labeled by probe **18** – the precursor protein or the individual saposins A-D – a closer look was taken at the identified peptides. An overview of the mouse prosaposin amino acid sequence and the labeled peptides (in bold) are displayed in Figure 10. Saposins A-D were each covered with at least one peptide. From this data it could not be established which Psap form was labeled, therefore a second pulldown experiment was performed to reproduce the results and expand the peptide coverage. Again, prosaposin was UV-enriched in this experiment (ratio +UV/-UV intensity = 7.25) and one peptide (ANEDVCQDCMK) was identified that was both part of the precursor protein and saposin B (Figure 10, bold). This may indicate that intact prosaposin is targeted by probe **18**. To confirm labeling of probe **18** to prosaposin, a pcDNA3.1 vector was generated containing prosaposin cDNA with a C-terminal FLAG-tag. Unfortunately, Psap overexpression in transfected Neuro-2a or HEK293T cells could not be confirmed by western blot.

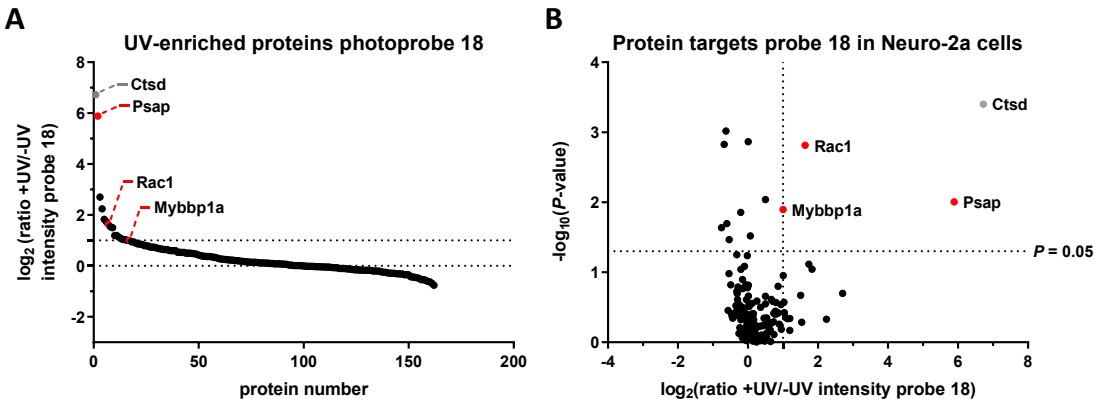

Figure 9. A) Waterfall plot showing UV enriched proteins of photoprobe **18** (20 μM) in Neuro-2a cells. **B**) Volcano plot displaying significant protein targets for probe **18** (20 μM). Red circles depict high confidence and grey circles low confidence targets. Data represent 3 biological replicates per condition. Cut-off values for protein target validation: unique peptides ≥ 2, ratio +UV (*heavy*)/+UV (*light*) probe **18** intensity 0.5 ≤ x ≤ 2, ratio +UV (*heavy*)/-UV (*light*) probe **18** intensity x ≥ 2. Statistically significant targets: $P < 0.05$ using Student's *t*-test (unpaired, two-tailed) and Benjamini-Hochberg correction with FDR of 25%.

Table 1. Protein targets of photoprobe **18** in Neuro-2a cells.

Name	Gene	MW (kDa)	Accession	Peptides		Ratio		*P*-value +UV/-UV Intensity	Function	Localization
				Total	Unique	+UV/+UV intensity	+UV/-UV intensity			
Cathepsin D	*Ctsd*	45	P18242	8	8	1.22	106	0.0003	Protease; cleaves prosaposin to saposins A-D[67]	Lysosome
Prosaposin	*Psap*	58	Q61207	9	9	1.21	59.2	0.0098	Neurotrophic factor[68]; saposins A-D are lipid binding proteins that activate sphingolipid hydrolases[66]	Cell membrane, lysosome
Ras-related C3 botulinum toxin substrate 1	*Rac1*	21	P63001	6	5	0.96	3.10	0.0015	GTPase[69]	Cell membrane
Myb-binding protein 1a (p160)	*Mybbp1a*	152	Q7TPV4	9	9	0.99	2.00	0.0127	Tumor suppressor[70,71]	Nucleus, cytosol

Cut-off values for protein target validation: unique peptides ≥ 2, ratio +UV (*heavy*)/+UV (*light*) probe **18** intensity $0.5 \leq x \leq 2$, ratio +UV (*heavy*)/-UV (*light*) probe **18** intensity $x \geq 2$. Statistically significant targets: $P < 0.05$ using Student's *t*-test (unpaired, two-tailed) and Benjamini-Hochberg correction with FDR of 25%.

1	MYALALFASLLATALTSPVQDPKTCSGGSAVLCRDVKTAVDCGAVKHCQQ	50	
51	MVWSKPTAKSLPCDICK-TVVTEAGNLLKDNATQEEILHYLEKTCEWIHDS	100	Sap A
101	SLSASCK-EVVDSYLPVILDMIKGEMSNPGEVCSALNLCQSLQEYLAEQNQ	151	
151	KQLESNKIPEVDMARVVAPFMSNIPLLLYPQDHPRSQPQPKANEDVCQDC	200	
201	MK-LVSDVQTAVKTNSSFIQGFVDHVKEDCDRLGPGVSDICKNYVDQYSEV	250	Sap B
251	CVQMLMHMQDQQPKEICVLAGFCNEVKRVPMKTLVPATETIKNILPALEM	300	
301	MDPYEQNLVQAHNVILCQTCQFVMNKFSELIVNNATEELLVKGLSNACAL	350	Sap C
351	LPDPARTKCQEVVGTFGPSLLDIFIHEVNPSSLCGVIGLCAARPELVEAL	400	
401	EQPAPAIVSALLKEPTPPKQPAQPKQSALPAHVPPQKNGGFCEVCKKLVL	450	
451	YLEHNLEKNSTKEEILAALEKGCSFLPDPYQKQCDDFVAEYEPLLLEILV	500	Sap D
501	EVMDPGFVCSKIGVCPSAYKLLLGTEKCVWGPSYWCQNMETAARCNAVDH	550	
551	CKRHVWN		

Figure 10. Amino acid sequence of full-length mouse prosaposin, showing the individual sequences of saposins A-D and the covered peptides (underlined) from two chemical proteomics experiments.

To summarize, four potential binding partners of NAPEs were identified using photoaffinity labeling. Considerable evidence suggests that the NAPE-prosaposin interaction could be an interesting topic for future studies in relation to neurodegeneration. Firstly, anionic phospholipids have been reported to stimulate the catalytic activity of saposin-mediated sphingolipid hydrolysis.[72] Furthermore, saposin B is involved in the breakdown of a class of sphingolipids called gangliosides. During brain ischemia and similar to NAPEs, certain gangliosides were found to be elevated in and confined to areas that show severe cell death.[73-75] The impact of anionic NAPE accumulation on sphingolipid metabolism is however not yet known. Secondly, prosaposin itself has been identified as a secreted and membrane-associated neurotrophic factor and a high-affinity ligand for the orphan G protein-coupled receptors GPR37 and GPR37L1.[76,77] Psap levels are also highly elevated in brain ischemia and prosaposin spinal cord infusion was found to be neuroprotective in a gerbil model of ischemia.[68,78,79] NAPEs could interfere with the trafficking of prosaposin from the ER to the lysosome where it undergoes proteolysis, thereby increasing the amount of secreted Psap and depleting the lysosomal pool of saposins A-D.[79]

Of the other protein targets, Rac1 also merits closer examination. Rac1 is a small guanosine triphosphatase (GTPase) in the Rho family of GTPases that regulates the rearrangement of the actin cytoskeleton and promotes phagocytosis.[69] During phagosome formation, Rac1 localizes to anionic phospholipids in the plasma membrane via its polybasic domain.[80] *N*-palmitoyl-PE (NPPE)-enriched liposomes decreased phagocytosis in mouse J774A.1 macrophages by inhibiting Rac1 activity, thereby terminating inflammation.[81] Furthermore, in a mouse model of brain ischemia, genetic deletion of *Rac1* showed to be neuroprotective.[82] Thus, Rac1 constitutes an interesting target to study with regard to the anti-inflammatory and/or neuroprotective effects of NAPEs.

7.4 Closing remarks

Selective and *in vivo* active inhibitors are essential for the elucidation of biological signaling networks and for the development of new drugs. The work described in this thesis provides new inhibitors (**LEI-301** and **LEI-401**), chemical tools and assays to study the NAE-producing enzymes NAPE-PLD and PLAAT2. Genetic KO models have not been able to fully illuminate the complexity of NAE biosynthesis, possibly due to long-term compensatory effects. By blocking these enzymes in an acute fashion, the contributory role of NAPE-PLD and PLAAT2 with regard to NAE formation can be assessed across specific cells and tissues. In addition, **LEI-301** and **LEI-401** are suitable starting points to investigate the biological consequences of depleting the NAE tone, which may be useful in pathological conditions such as obesity, metabolic syndrome, chronic liver disease and cancer.

Acknowledgements

Bobby Florea, Peter van Veelen and Arnoud de Ru are kindly acknowledged for performing proteomics measurements.

7.4 Experimental section

Cell culture

Neuro-2a cells (ATCC) were cultured at 37 ^{o}C and 7% CO_2 in DMEM (Sigma Aldrich, D6546) with GlutaMax, penicillin (100 μg/ml), streptomycin (100 μg/ml) and 10% fetal calf serum. Cells were passaged twice a week to appropriate confluence by thorough pipetting.

Gel-based photoaffinity labeling

Neuro-2a cells were seeded in a 12-well plate (750,000 cells per well) 1 day before treatment. The cells were treated with the photoprobes **16-22** (500x in DMSO, final concentration: 20 μM) in medium + serum (0.30 mL per well) for 30 min at 37 °C. The medium was aspirated and the cells were covered with PBS (0.15 mL per well), followed by UV irradiation using a Caprobox™ (10 min, 350 nm, 4 °C) or kept in the dark as a control. The cells were harvested into 1.5 mL epps with cold PBS and centrifuged (10 min, 2000 rpm, 4 °C). The PBS was removed and the cells were flash frozen with liquid N_2 (cells pellets can be stored at -80 °C). The cells were lysed with lysis buffer (30 μL, 20 mM HEPES pH 7.2, 0.25 M sucrose, 1 mM $MgCl_2$, benzonase 25 U/mL) followed by pipetting up and down and incubating for 30 min on ice. Protein concentrations were measured using a Bradford assay (Bio-Rad), and cell lysates were diluted to 2 μg/μL with lysis buffer. 18 μg cell lysate (9 μL) was then clicked with Cy5-N_3 using a click mix (1 μL per sample, final concentrations: 1 mM $CuSO_4$, 6 mM sodium ascorbate, 0.2 mM tris(3-hydroxypropyltriazolylmethyl)-amine (THPTA), 2 μM Cy5-N_3) for 1 h at rt (Note: it is important to separately prepare the click mix first with $CuSO_4$ and sodium ascorbate, until a yellow color change is observed). Samples were denatured with 4x Laemmli buffer (3.33 μL, stock concentration: 240 mM Tris-HCl pH 6.8, 8% w/v SDS, 40% v/v glycerol, 5% v/v β-mercaptoethanol, 0.04% v/v bromophenol blue) and incubated for 30 min at rt. The samples were resolved by SDS-PAGE (10% acrylamide gel) at 180 V for 75 min, after which the gels were imaged at Cy3 and Cy5 channels (605/50 and 695/55 filters, respectively) on a ChemiDoc™ Imaging System (Bio-Rad). Gels were stained with Coomassie as a loading control.

Chemical proteomics-based photoaffinity labeling

10^7 Neuro-2a cells were seeded in a 10 cm dish 1 day before treatment, three replicates per group. Cells were treated with photoprobe **18** (500x in DMSO, final concentration: 20 μM) in medium + serum (4 mL per dish) for 30 min at 37 °C. The medium was aspirated and the cells were covered with PBS (1.5 mL per dish), followed by UV irradiation using a Caprobox™ (10 min, 350 nm, 4 °C) or kept in the dark as a control. The cells were harvested into 15 mL tubes with cold PBS and centrifuged (10 min, 2000 rpm, 4 °C). The supernatant was removed and the cells were washed with PBS (1 x 10 mL) and centrifuged (10 min, 2000 rpm, 4 °C). The PBS was removed and the cell pellets were flash frozen with liquid N_2 (cell pellets can be stored at -80 °C for later use). The cells were lysed with lysis buffer (200 μL, 20 mM HEPES pH 7.2, 0.25 M sucrose, 1 mM $MgCl_2$, benzonase 25 U/mL) followed by probe sonication (10% amplitude, 4 x 2.5 s) and incubation for 30 min on ice. The lysates were centrifuged (90 min, 30,000 *g*, 4 °C) giving the cytosol fraction (supernatant). The membrane fraction (pellet) was resuspended in storage buffer (250 μL, 20 mM HEPES pH 7.2) and homogenized by probe sonication (10% amplitude, 4 x 2.5 s). Protein concentrations were determined using a Bradford assay (Bio-Rad) and cell lysates were diluted to 2 μg/μL with lysis buffer.

From here the quantitative chemical proteomics protocol using dimethyl labeling was followed as previously described with small alterations.[83] 225 μL cytosol or membrane lysate (450 μg) was clicked with biotin-N_3 (Sigma Aldrich, 762024) using a click mix (25 μL per sample, final concentrations: 1 mM $CuSO_4$, 6 mM sodium ascorbate, 0.2 mM tris(3-hydroxypropyltriazolylmethyl)amine (THPTA), 100 μM biotin-N_3) for 1 h at rt (Note: it is important to separately prepare the click mix first with $CuSO_4$ and sodium ascorbate, until a yellow color change is observed). Proteins were precipitated using chloroform (166 μL), methanol (666 μL) and MilliQ (416 μL). Samples were centrifuged (10 min, 1,500 *g*) and the solvents were carefully removed. Methanol (600 μL) was added and the proteins were resuspended using a probe sonicator (30% amplitude, 10 s). After centrifugation (5 min, 18,400 *g*) the supernatant was removed and the samples were resuspended in urea buffer (500 μL, 6 M urea, 250 mM NH_4HCO_3) by pipetting up and down. 1 M DTT (5 μL, final concentration 10 mM) was added and the samples were incubated with shaking (15 min, 600 rpm, 65 °C). After cooling to rt, 0.5 M iodoacetamide (40 μL, final concentration 40 mM) was added and incubated in the dark with shaking (30 min, 600 rpm, 20 °C). Next, 10% SDS (140 μL, final concentration 2%) was added and incubated with shaking (5 min, 600 rpm, 65 °C). For 18 samples, 1.8 mL of avidin agarose beads (Sigma-

Aldrich, A9207) was divided over three 15 mL tubes and washed with PBS (3 x 10 mL). The beads in each tube were resuspended in PBS (6 mL) and divided over 18 tubes (1 mL each). To each tube was added the denatured sample and PBS (4.5 mL) and the tubes were rotated with an overhead shaker at rt for 2 h. After centrifugation (2 min, 2,500 *g*) and removal of the supernatant, the beads were consecutively washed with 0.5% SDS in PBS (w/v, 6 mL) and PBS (3 x 6 mL), each time centrifuging (2 min, 2,500 *g*). The beads were transferred to a 1.5 mL low binding epp (Sarstedt, 72.706.600) with on-bead digestion buffer (200 μL, 100 mM Tris pH 8.0, 100 mM NaCl, 1 mM $CaCl_2$, 2% v/v acetonitrile) and to each sample was added 1 μL trypsin solution (0.5 μg/μL trypsin (Promega, V5111), 0.1 mM HCl). Proteins were digested with vigorous shaking overnight (950 rpm, 37 ^{o}C). Formic acid (10 μL) was added to each sample and the beads were filtered off by centrifugation (2.5 min, 600 *g*) using a biospin column (Bio-Rad, 7326204), the flow-through was collected in a 2 mL epp.

Tryptic digests were desalted and treated with heavy or light isotopically labeled formaldehyde using StageTips.[84] The samples were treated according to the following steps:

Step	**Treatment**	**Centrifugation***
Conditioning 1	Methanol (50 μL)	2 min, 600 *g*
Conditioning 2	StageTip solution B (50 μL)	2 min, 600 *g*
Conditioning 3	StageTip solution A (50 μL)	2 min, 600 *g*
Loading	Load samples on StageTips	2.5 min, 800 *g*
Washing	StageTip solution A (100 μL)	2.5 min, 800 *g*
Dimethyl labeling	Heavy or light reagent mix (5 x 20 μL)	5.0 min, 400 *g*
Washing	StageTip solution A (100 μL)	2.5 min, 800 *g*
Transfer	Transfer StageTip to new 1.5 mL low binding epp	
Elution	StageTip solution B (100 μL)	2.5 min, 800 *g*

* *Indication speed.*

StageTip solution A: 80% v/v acetonitrile, 0.5% v/v formic acid in MilliQ.
StageTip solution B: 0.5% v/v formic acid in MilliQ.
Heavy reagent mix: 50 mM phosphate buffer pH 7.5, 2% v/v CD_2O, 30 mM $NaBH_3CN$.
Light reagent mix: 50 mM phosphate buffer pH 7.5, 2% v/v CH_2O, 30 mM $NaBH_3CN$.

The solvents were evaporated to dryness in a SpeedVac concentrator (3 h, 45 ^{o}C). Samples were reconstituted in LC-MS solution (50 μL, 3% v/v acetonitrile, 0.1% v/v formic acid in MilliQ). Samples were combined in a 1:1 ratio, affording 4 sample groups:

- Heavy (+UV) + light (+UV) labeled membrane fraction (quality control)
- Heavy (+UV) + light (+UV) labeled cytosol fraction (quality control)
- Heavy (+UV) + light (-UV) labeled membrane fraction (UV-enrichment)
- Heavy (+UV) + light (-UV) labeled cytosol fraction (UV-enrichment)

Tryptic peptides were analyzed on a Surveyor nanoLC system (Thermo) hyphenated to a LTQ-Orbitrap mass spectrometer (ThermoFisher). Briefly, emitter, trap and analytical column (C18, 120 Å) were purchased from Nanoseparations (Nieuwkoop, The Netherlands) and mobile phases (A: 0.1% formic acid/H_2O, B: 0.1% formic acid/ACN) were made with ULC/MS grade solvents (Biosolve). General mass spectrometric conditions were: electrospray voltage of 1.8-2.5 kV, no sheath and auxiliary gas flow, capillary voltage 40 V, tube lens voltage 155 V and ion transfer tube temperature 150 ^{o}C. Polydimethylcyclosiloxane (m/z = 445.12002) and dioctyl phthalate ions (m/z = 391.28429) from the milieu were used as lock mass. Some 10 μL of the samples was pressure loaded on the trap column for 5 min with a 10 μL/min flow and separated with a gradient of

35 min 5%-30% B, 15 min 30%-60% B, 5 min A at a flow of 300 μL/min split to 250 nL/min by the LTQ divert valve. Full MS scans (300-2000 m/z) acquired at high mass resolution (60,000 at 400 m/z, maximum injection time 1000 ms, AGC 106) in the Orbitrap was followed by three MS/MS fragmentations in the LTQ linear ion trap (AGC 5 x 103, maximum injection time 120 ms) from the three most abundant ions. MS/MS settings were: collision gas pressure 1.3 mT, normalized collision energy 35%, ion selection threshold of 750 counts, activation q = 0.25 and activation time 30 ms. Ions of z < 2 or unassigned were not analyzed and fragmented precursor ions were measured twice within 10 s and were dynamically excluded for 60 s.

Data analysis was performed using Maxquant with acetylation (protein *N*-terminus) and oxidation (M) as variable modifications. The false discovery rate was set at 1% and the peptides were screened against mouse proteome (Uniprot). Proteins were designated as probe **18** targets according to the following cut-offs: unique peptides ≥ 2, ratio +UV (*heavy*)/+UV (*light*) probe **18** intensity 0.5 ≤ x ≤ 2, ratio +UV (*heavy*)/-UV (*light*) probe **18** intensity x ≥ 2. Statistic testing: $P < 0.05$ using Student's *t*-test (unpaired, two-tailed) and Benjamini-Hochberg correction with FDR of 25%.

References

1. Devane, W., Hanus, L., Breuer, A., Pertwee, R., Stevenson, L., Griffin, G., Gibson, D., Mandelbaum, A., Etinger, A. & Mechoulam, R. Isolation and structure of a brain constituent that binds to the cannabinoid receptor. *Science* **258**, 1946-1949 (1992).
2. Stelt, M.v.d. & Marzo, V.D. Endovanilloids. *European Journal of Biochemistry* **271**, 1827-1834 (2004).
3. Cravatt, B.F., Demarest, K., Patricelli, M.P., Bracey, M.H., Giang, D.K., Martin, B.R. & Lichtman, A.H. Supersensitivity to anandamide and enhanced endogenous cannabinoid signaling in mice lacking fatty acid amide hydrolase. *Proceedings of the National Academy of Sciences* **98**, 9371-9376 (2001).
4. Williams, C.M. & Kirkham, T.C. Anandamide induces overeating: mediation by central cannabinoid (CB_1) receptors. *Psychopharmacology* **143**, 315-317 (1999).
5. Wang, H., Xie, H., Guo, Y., Zhang, H., Takahashi, T., Kingsley, P.J., Marnett, L.J., Das, S.K., Cravatt, B.F. & Dey, S.K. Fatty acid amide hydrolase deficiency limits early pregnancy events. *The Journal of Clinical Investigation* **116**, 2122-2131 (2006).
6. Eljaschewitsch, E., Witting, A., Mawrin, C., Lee, T., Schmidt, P.M., Wolf, S., Hoertnagl, H., Raine, C.S., Schneider-Stock, R., Nitsch, R. & Ullrich, O. The endocannabinoid anandamide protects neurons during CNS inflammation by induction of MKP-1 in microglial cells. *Neuron* **49**, 67-79 (2006).
7. Morena, M., Roozendaal, B., Trezza, V., Ratano, P., Peloso, A., Hauer, D., Atsak, P., Trabace, L., Cuomo, V., McGaugh, J.L., Schelling, G. & Campolongo, P. Endogenous cannabinoid release within prefrontal-limbic pathways affects memory consolidation of emotional training. *Proceedings of the National Academy of Sciences* **111**, 18333-18338 (2014).
8. Gobbi, G., Bambico, F.R., Mangieri, R., Bortolato, M., Campolongo, P., Solinas, M., Cassano, T., Morgese, M.G., Debonnel, G., Duranti, A., Tontini, A., Tarzia, G., Mor, M., Trezza, V., Goldberg, S.R., Cuomo, V. & Piomelli, D. Antidepressant-like activity and modulation of brain monoaminergic transmission by blockade of anandamide hydrolysis. *Proceedings of the National Academy of Sciences* **102**, 18620-18625 (2005).
9. Kathuria, S., Gaetani, S., Fegley, D., Valiño, F., Duranti, A., Tontini, A., Mor, M., Tarzia, G., Rana, G.L., Calignano, A., Giustino, A., Tattoli, M., Palmery, M., Cuomo, V. & Piomelli, D. Modulation of anxiety through blockade of anandamide hydrolysis. *Nature Medicine* **9**, 76 (2002).
10. Fanelli, F., Mezzullo, M., Repaci, A., Belluomo, I., Ibarra Gasparini, D., Di Dalmazi, G., Mastroroberto, M., Vicennati, V., Gambineri, A., Morselli-Labate, A.M., Pasquali, R. & Pagotto, U. Profiling plasma *N*-acylethanolamine levels and their ratios as a biomarker of obesity and dysmetabolism. *Molecular Metabolism* **14**, 82-94 (2018).

11. Bowles, N.P., Karatsoreos, I.N., Li, X., Vemuri, V.K., Wood, J.-A., Li, Z., Tamashiro, K.L.K., Schwartz, G.J., Makriyannis, A.M., Kunos, G., Hillard, C.J., McEwen, B.S. & Hill, M.N. A peripheral endocannabinoid mechanism contributes to glucocorticoid-mediated metabolic syndrome. *Proceedings of the National Academy of Sciences* **112**, 285-290 (2015).
12. Mukhopadhyay, B., Schuebel, K., Mukhopadhyay, P., Cinar, R., Godlewski, G., Xiong, K., Mackie, K., Lizak, M., Yuan, Q., Goldman, D. & Kunos, G. Cannabinoid receptor 1 promotes hepatocellular carcinoma initiation and progression through multiple mechanisms. *Hepatology* **61**, 1615-1626 (2015).
13. Masoodi, M., Lee, E., Eiden, M., Bahlo, A., Shi, Y., Ceddia, R.B., Baccei, C., Prasit, P. & Spaner, D.E. A role for oleoylethanolamide in chronic lymphocytic leukemia. *Leukemia* **28**, 1381 (2014).
14. Caraceni, P., Viola, A., Piscitelli, F., Giannone, F., Berzigotti, A., Cescon, M., Domenicali, M., Petrosino, S., Giampalma, E., Riili, A., Grazi, G., Golfieri, R., Zoli, M., Bernardi, M. & Di Marzo, V. Circulating and hepatic endocannabinoids and endocannabinoid-related molecules in patients with cirrhosis. *Liver International* **30**, 816-825 (2010).
15. Tam, J., Hinden, L., Drori, A., Udi, S., Azar, S. & Baraghithy, S. The therapeutic potential of targeting the peripheral endocannabinoid/CB_1 receptor system. *European Journal of Internal Medicine* **49**, 23-29 (2018).
16. Hussain, Z., Uyama, T., Tsuboi, K. & Ueda, N. Mammalian enzymes responsible for the biosynthesis of *N*-acylethanolamines. *Biochimica et Biophysica Acta (BBA) - Molecular and Cell Biology of Lipids* **1862**, 1546-1561 (2017).
17. Leung, D., Saghatelian, A., Simon, G.M. & Cravatt, B.F. Inactivation of *N*-acyl phosphatidylethanolamine phospholipase D reveals multiple mechanisms for the biosynthesis of endocannabinoids. *Biochemistry* **45**, 4720-4726 (2006).
18. Tsuboi, K., Okamoto, Y., Ikematsu, N., Inoue, M., Shimizu, Y., Uyama, T., Wang, J., Deutsch, D.G., Burns, M.P., Ulloa, N.M., Tokumura, A. & Ueda, N. Enzymatic formation of *N*-acylethanolamines from *N*-acylethanolamine plasmalogen through *N*-acylphosphatidylethanolamine-hydrolyzing phospholipase D-dependent and -independent pathways. *Biochimica et Biophysica Acta (BBA) - Molecular and Cell Biology of Lipids* **1811**, 565-577 (2011).
19. Leishman, E., Mackie, K., Luquet, S. & Bradshaw, H.B. Lipidomics profile of a NAPE-PLD KO mouse provides evidence of a broader role of this enzyme in lipid metabolism in the brain. *Biochimica et Biophysica Acta (BBA) - Molecular and Cell Biology of Lipids* **1861**, 491-500 (2016).
20. Lapinsky, D.J. & Johnson, D.S. Recent developments and applications of clickable photoprobes in medicinal chemistry and chemical biology. *Future Medicinal Chemistry* **7**, 2143-2171 (2015).
21. Smith, D.A., Beaumont, K., Maurer, T.S. & Di, L. Relevance of half-life in drug design. *Journal of Medicinal Chemistry* **61**, 4273-4282 (2018).
22. Hopkins, A.L., Keserü, G.M., Leeson, P.D., Rees, D.C. & Reynolds, C.H. The role of ligand efficiency metrics in drug discovery. *Nature Reviews Drug Discovery* **13**, 105 (2014).
23. Meanwell, N.A. Fluorine and fluorinated motifs in the design and application of bioisosteres for drug design. *Journal of Medicinal Chemistry* **61**, 5822-5880 (2018).
24. Bagal, S.K. & Bungay, P.J. Minimizing drug exposure in the CNS while maintaining good oral absorption. *ACS Medicinal Chemistry Letters* **3**, 948-950 (2012).
25. Ogasawara, D., Deng, H., Viader, A., Baggelaar, M.P., Breman, A., den Dulk, H., van den Nieuwendijk, A.M.C.H., Soethoudt, M., van der Wel, T., Zhou, J., Overkleeft, H.S., Sanchez-Alavez, M., Mori, S., Nguyen, W., Conti, B., Liu, X., Chen, Y., Liu, Q.-s., Cravatt, B.F. & van der Stelt, M. Rapid and profound rewiring of brain lipid signaling networks by acute diacylglycerol lipase inhibition. *Proceedings of the National Academy of Sciences* **113**, 26 (2016).
26. Maccarrone, M., Rossi, S., Bari, M., De Chiara, V., Fezza, F., Musella, A., Gasperi, V., Prosperetti, C., Bernardi, G., Finazzi-Agrò, A., Cravatt, B.F. & Centonze, D. Anandamide inhibits metabolism and physiological actions of 2-arachidonoylglycerol in the striatum. *Nature Neuroscience* **11**, 152 (2008).

27. Wright, M.H. & Sieber, S.A. Chemical proteomics approaches for identifying the cellular targets of natural products. *Natural Product Reports* **33**, 681-708 (2016).
28. Flaxman, H.A. & Woo, C.M. Mapping the small molecule interactome by mass spectrometry. *Biochemistry* **57**, 186-193 (2018).
29. Smith, E. & Collins, I. Photoaffinity labeling in target- and binding-site identification. *Future Medicinal Chemistry* **7**, 159-183 (2015).
30. Yang, Y., Fonović, M. & Verhelst, S.H.L. Cleavable linkers in chemical proteomics applications, in *Activity-Based Proteomics: Methods and Protocols*. (eds. H.S. Overkleeft & B.I. Florea) 185-203 (Springer New York, New York, NY; 2017).
31. van der Stelt, M., Hansen, H.H., Veldhuis, W.B., Bär, P.R., Nicolay, K., Veldink, G.A., Vliegenthart, J.F.G. & Hansen, H.S. Biosynthesis of endocannabinoids and their modes of action in neurodegenerative diseases. *Neurotoxicity Research* **5**, 183-199 (2003).
32. Wang, J. & Ueda, N. Biology of endocannabinoid synthesis system. *Prostaglandins & Other Lipid Mediators* **89**, 112-119 (2009).
33. Uyama, T., Ikematsu, N., Inoue, M., Shinohara, N., Jin, X.-H., Tsuboi, K., Tonai, T., Tokumura, A. & Ueda, N. Generation of *N*-acylphosphatidylethanolamine by members of the phospholipase A/acyltransferase (PLA/AT) family. *Journal of Biological Chemistry* **287**, 31905-31919 (2012).
34. Zhou, J., Mock, E.D., Martella, A., Kantae, V., Di, X., Burggraaff, L., Baggelaar, M.P., Al-Ayed, K., Bakker, A., Florea, B.I., Grimm, S.H., den Dulk, H., Li, C.T., Mulder, L., Overkleeft, H.S., Hankemeier, T., van Westen, G.J.P. & van der Stelt, M. Activity-based protein profiling identifies α-ketoamides as inhibitors for phospholipase A_2 group XVI. *ACS Chemical Biology* **14**, 164-169 (2019).
35. Fischl, W., Whittaker, M., Yarnold, C.J., Pons, J.-F., Kerry, M.A., Amouzegh, P.L., Morao, I., Ingram, P.N. & Chudyk, E.I., Vol. WO2018050631A1.
36. Golczak, M., Kiser, P.D., Sears, A.E., Lodowski, D.T., Blaner, W.S. & Palczewski, K. Structural basis for the acyltransferase activity of lecithin:retinol acyltransferase-like proteins. *J Biol Chem* **287**, 23790-23807 (2012).
37. Pang, X.-Y., Cao, J., Addington, L., Lovell, S., Battaile, K.P., Zhang, N., Rao, J.L.U.M., Dennis, E.A. & Moise, A.R. Structure/function relationships of adipose phospholipase A_2 containing a Cys-His-His catalytic triad. *Journal of Biological Chemistry* **287**, 35260-35274 (2012).
38. Baggelaar, M.P., Janssen, F.J., van Esbroeck, A.C.M., den Dulk, H., Allara, M., Hoogendoorn, S., McGuire, R., Florea, B.I., Meeuwenoord, N., van den Elst, H., van der Marel, G.A., Brouwer, J., Di Marzo, V., Overkleeft, H.S. & van der Stelt, M. Development of an activity-based probe and in silico design reveal highly selective inhibitors for diacylglycerol lipase-alpha in brain. *Angew. Chem.-Int. Edit.* **52**, 12081-12085 (2013).
39. Mulder, M.P.C., Witting, K., Berlin, I., Pruneda, J.N., Wu, K.-P., Chang, J.-G., Merkx, R., Bialas, J., Groettrup, M., Vertegaal, A.C.O., Schulman, B.A., Komander, D., Neefjes, J., El Oualid, F. & Ovaa, H. A cascading activity-based probe sequentially targets E1–E2–E3 ubiquitin enzymes. *Nature Chemical Biology* **12**, 523 (2016).
40. Verdoes, M., Oresic Bender, K., Segal, E., van der Linden, W.A., Syed, S., Withana, N.P., Sanman, L.E. & Bogyo, M. Improved quenched fluorescent probe for imaging of cysteine cathepsin activity. *Journal of the American Chemical Society* **135**, 14726-14730 (2013).
41. Sanman, L.E. & Bogyo, M. Activity-based profiling of proteases. *Annual Review of Biochemistry* **83**, 249-273 (2014).
42. Leyva, M.J., DeGiacomo, F., Kaltenbach, L.S., Holcomb, J., Zhang, N., Gafni, J., Park, H., Lo, D.C., Salvesen, G.S., Ellerby, L.M. & Ellman, J.A. Identification and evaluation of small molecule pan-caspase inhibitors in Huntington's disease models. *Chemistry & Biology* **17**, 1189-1200 (2010).
43. Shyu, R.-Y., Hsieh, Y.-C., Tsai, F.-M., Wu, C.-C. & Jiang, S.-Y. Cloning and functional characterization of the HRASLS2 gene. *Amino Acids* **35**, 129-137 (2008).

44. Uyama, T., Jin, X.-H., Tsuboi, K., Tonai, T. & Ueda, N. Characterization of the human tumor suppressors TIG3 and HRASLS2 as phospholipid-metabolizing enzymes. *Biochimica et Biophysica Acta (BBA) - Molecular and Cell Biology of Lipids* **1791**, 1114-1124 (2009).
45. Piomelli, D. A fatty gut feeling. *Trends in Endocrinology & Metabolism* **24**, 332-341 (2013).
46. van Eenige, R., van der Stelt, M., Rensen, P.C.N. & Kooijman, S. Regulation of adipose tissue metabolism by the endocannabinoid system. *Trends in Endocrinology & Metabolism* **29**, 326-337 (2018).
47. Coulon, D., Faure, L., Salmon, M., Wattelet, V. & Bessoule, J.-J. Occurrence, biosynthesis and functions of *N*-acylphosphatidylethanolamines (NAPE): Not just precursors of *N*-acylethanolamines (NAE). *Biochimie* **94**, 75-85 (2012).
48. Wellner, N., Diep, T.A., Janfelt, C. & Hansen, H.S. *N*-Acylation of phosphatidylethanolamine and its biological functions in mammals. *Biochimica et Biophysica Acta (BBA) - Molecular and Cell Biology of Lipids* **1831**, 652-662 (2013).
49. Domingo, J.C., Mora, M. & Africa de Madariaga, M. Role of headgroup structure in the phase behaviour of *N*-acylethanolamine phospholipids: hydrogen-bonding ability and headgroup size. *Chemistry and Physics of Lipids* **69**, 229-240 (1994).
50. Swamy, M.J., Tarafdar, P.K. & Kamlekar, R.K. Structure, phase behaviour and membrane interactions of *N*-acylethanolamines and *N*-acylphosphatidylethanolamines. *Chemistry and Physics of Lipids* **163**, 266-279 (2010).
51. Shangguan, T., Pak, C.C., Ali, S., Janoff, A.S. & Meers, P. Cation-dependent fusogenicity of an *N*-acyl phosphatidylethanolamine. *Biochimica et Biophysica Acta (BBA) - Biomembranes* **1368**, 171-183 (1998).
52. Mora, M., Mir, F., de Madariaga, M.A. & Sagrista, M.L. Aggregation and fusion of vesicles composed of *N*-palmitoyl derivatives of membrane phospholipids. *Lipids* **35**, 513-524 (2000).
53. Epps, D.E., Natarajan, V., Schmid, P.C. & Schmid, H.H.O. Accumulation of *N*-acylethanolamine glycerophospholipids in infarcted myocardium. *Biochimica et Biophysica Acta (BBA) - Lipids and Lipid Metabolism* **618**, 420-430 (1980).
54. Natarajan, V., Schmid, P.C. & Schmid, H.H.O. *N*-Acylethanolamine phospholipid metabolism in normal and ischemic rat brain. *Biochimica et Biophysica Acta (BBA) - Lipids and Lipid Metabolism* **878**, 32-41 (1986).
55. Moesgaard, B., Petersen, G., Jaroszewski, J.W. & Hansen, H.S. Age dependent accumulation of *N*-acyl-ethanolamine phospholipids in ischemic rat brain: a 31P NMR and enzyme activity study. *Journal of Lipid Research* **41**, 985-990 (2000).
56. Hansen, H.H., Ikonomidou, C., Bittigau, P., Hansen, S.H. & Hansen, H.S. Accumulation of the anandamide precursor and other *N*-acylethanolamine phospholipids in infant rat models of *in vivo* necrotic and apoptotic neuronal death. *Journal of Neurochemistry* **76**, 39-46 (2001).
57. Moesgaard, B., Hansen, H.H., Hansen, S.L., Hansen, S.H., Petersen, G. & Hansen, H.S. Brain levels of *N*-acylethanolamine phospholipids in mice during pentylenetetrazol-induced seizure. *Lipids* **38**, 387-390 (2003).
58. Janfelt, C., Wellner, N., Leger, P.-L., Kokesch-Himmelreich, J., Hansen, S.H., Charriaut-Marlangue, C. & Hansen, H.S. Visualization by mass spectrometry of 2-dimensional changes in rat brain lipids, including *N*-acylphosphatidylethanolamines, during neonatal brain ischemia. *The FASEB Journal* **26**, 2667-2673 (2012).
59. Basit, A., Pontis, S., Piomelli, D. & Armirotti, A. Ion mobility mass spectrometry enhances low-abundance species detection in untargeted lipidomics. *Metabolomics* **12**, 50 (2016).
60. Rawyler, A.J. & Braendle, R.A. *N*-Acylphosphatidylethanolamine accumulation in potato cells upon energy shortage caused by anoxia or respiratory inhibitors. *Plant Physiology* **127**, 240-251 (2001).

61. Zhang, C. & Tian, S. Peach fruit acquired tolerance to low temperature stress by accumulation of linolenic acid and *N*-acylphosphatidylethanolamine in plasma membrane. *Food Chemistry* **120**, 864-872 (2010).
62. Pongracz, K. & Gryaznov, S. Oligonucleotide N3'→P5' thiophosphoramidates: synthesis and properties. *Tetrahedron Letters* **40**, 7661-7664 (1999).
63. Hsu, J.-L., Huang, S.-Y., Chow, N.-H. & Chen, S.-H. Stable-isotope dimethyl labeling for quantitative proteomics. *Analytical Chemistry* **75**, 6843-6852 (2003).
64. Cox, J. & Mann, M. MaxQuant enables high peptide identification rates, individualized p.p.b.-range mass accuracies and proteome-wide protein quantification. *Nature Biotechnology* **26**, 1367 (2008).
65. Kleiner, P., Heydenreuter, W., Stahl, M., Korotkov, V.S. & Sieber, S.A. A whole proteome inventory of background photocrosslinker binding. *Angewandte Chemie International Edition* **56**, 1396-1401 (2017).
66. Kolter, T. & Sandhoff, K. Lysosomal degradation of membrane lipids. *FEBS Letters* **584**, 1700-1712 (2010).
67. Hiraiwa, M., Martin, B.M., Kishimoto, Y., Conner, G.E., Tsuji, S. & O'Brien, J.S. Lysosomal proteolysis of prosaposin, the precursor of saposins (sphingolipid activator proteins): its mechanism and inhibition by ganglioside. *Archives of Biochemistry and Biophysics* **341**, 17-24 (1997).
68. Meyer, R.C., Giddens, M.M., Coleman, B.M. & Hall, R.A. The protective role of prosaposin and its receptors in the nervous system. *Brain Research* **1585**, 1-12 (2014).
69. Payapilly, A. & Malliri, A. Compartmentalisation of RAC1 signalling. *Current Opinion in Cell Biology* **54**, 50-56 (2018).
70. Mori, S., Bernardi, R., Laurent, A., Resnati, M., Crippa, A., Gabrieli, A., Keough, R., Gonda, T.J. & Blasi, F. Myb-binding protein 1a (MYBBP1A) is essential for early embryonic development, controls cell cycle and mitosis, and acts as a tumor suppressor. *PLOS ONE* **7**, e39723 (2012).
71. Akaogi, K., Ono, W., Hayashi, Y., Kishimoto, H. & Yanagisawa, J. MYBBP1A suppresses breast cancer tumorigenesis by enhancing the p53 dependent anoikis. *BMC Cancer* **13**, 65 (2013).
72. Abdul-Hammed, M., Breiden, B., Schwarzmann, G. & Sandhoff, K. Lipids regulate the hydrolysis of membrane bound glucosylceramide by lysosomal β-glucocerebrosidase. *Journal of Lipid Research* **58**, 563-577 (2017).
73. Trindade, V.M.T., Daniotti, J.L., Raimondi, L., Chazan, R., Netto, C.A. & Maccioni, H.J.F. Effects of neonatal hypoxia/ischemia on ganglioside expression in the rat hippocampus. *Neurochemical Research* **26**, 591-597 (2001).
74. Whitehead, S.N., Chan, K.H.N., Gangaraju, S., Slinn, J., Li, J. & Hou, S.T. Imaging mass spectrometry detection of gangliosides species in the mouse brain following transient focal cerebral ischemia and long-term recovery. *PLOS ONE* **6**, e20808 (2011).
75. Luptakova, D., Baciak, L., Pluhacek, T., Skriba, A., Sediva, B., Havlicek, V. & Juranek, I. Membrane depolarization and aberrant lipid distributions in the neonatal rat brain following hypoxic-ischaemic insult. *Scientific Reports* **8**, 6952 (2018).
76. O'Brien, J.S., Carson, G.S., Seo, H.C., Hiraiwa, M. & Kishimoto, Y. Identification of prosaposin as a neurotrophic factor. *Proceedings of the National Academy of Sciences* **91**, 9593-9596 (1994).
77. Meyer, R.C., Giddens, M.M., Schaefer, S.A. & Hall, R.A. GPR37 and GPR37L1 are receptors for the neuroprotective and glioprotective factors prosaptide and prosaposin. *Proceedings of the National Academy of Sciences* **110**, 9529-9534 (2013).
78. Sano, A., Matsuda, S., Wen, T.C., Kotani, Y., Kondoh, K., Ueno, S., Kakimoto, Y., Yoshimura, H. & Sakanaka, M. Protection by prosaposin against ischemia-induced learning disability and neuronal loss. *Biochemical and Biophysical Research Communications* **204**, 994-1000 (1994).
79. Costain, W.J., Haqqani, A.S., Rasquinha, I., Giguere, M.-S., Slinn, J., Zurakowski, B. & Stanimirovic, D.B. Proteomic analysis of synaptosomal protein expression reveals that cerebral ischemia alters lysosomal Psap processing. *Proteomics* **10**, 3272-3291 (2010).

80. Magalhaes, M.A.O. & Glogauer, M. Pivotal advance: phospholipids determine net membrane surface charge resulting in differential localization of active Rac1 and Rac2. *Journal of Leukocyte Biology* **87**, 545-555 (2010).
81. Ichiki, M., Sugimoto, N., Ueda, N., Okamoto, Y., Takuwa, Y., Nakanishi, Y. & Shiratsuchi, A. Inhibitory effect of *N*-palmitoylphosphatidylethanolamine on macrophage phagocytosis through inhibition of Rac1 and Cdc42. *The Journal of Biochemistry* **145**, 43-50 (2008).
82. Karabiyik, C., Fernandes, R., Figueiredo, F.R., Socodato, R., Brakebusch, C., Lambertsen, K.L., Relvas, J.B. & Santos, S.D. Neuronal Rho GTPase Rac1 elimination confers neuroprotection in a mouse model of permanent ischemic stroke. *Brain Pathology* **28**, 569-580 (2018).
83. Baggelaar, M.P., Chameau, P.J.P., Kantae, V., Hummel, J., Hsu, K.L., Janssen, F., van der Wel, T., Soethoudt, M., Deng, H., den Dulk, H., Allara, M., Florea, B.I., Di Marzo, V., Wadman, W.J., Kruse, C.G., Overkleeft, H.S., Hankemeier, T., Werkman, T.R., Cravatt, B.F. & van der Stelt, M. Highly selective, reversible inhibitor identified by comparative chemoproteomics modulates diacylglycerol lipase activity in neurons. *Journal of the American Chemical Society* **137**, 8851-8857 (2015).
84. Rappsilber, J., Mann, M. & Ishihama, Y. Protocol for micro-purification, enrichment, pre-fractionation and storage of peptides for proteomics using StageTips. *Nature Protocols* **2**, 1896 (2007).